Draft version October 20, 2023
Typeset using LaTeX **twocolumn** style in AASTeX631

# The Effect of Donor Star Rejuvenation on Common Envelope Evolution

Camille Landri [1], Paul Ricker [2], Mathieu Renzo [3,4], Alejandro Vigna-Gómez [5] and ...[6]

[1] *Institute of Theoretical Physics, Faculty of Mathematics and Physics, Charles University, V Holešovickách 2, CZ-180 00 Praha 8, Czech Republic*

[2] *Department of Astronomy, University of Illinois, 1002 W. Green St., Urbana IL 61801*

[3] *Center for Computational Astrophysics, Flatiron Institute, 162 5th Ave, New York, NY 10010, USA*

[4] *Steward Observatory, University of Arizona, 933 N. Cherry Ave., Tucson, AZ 85721, USA*

[5] *Max-Planck-Institut für Astrophysik, Karl-Schwarzschild-Str. 1, D-85748 Garching, Germany*

[6] ...

## ABSTRACT

We report on the progress made on the research project carried during the MPA Kavli Summer Program for Astrophysics 2023, which is centered around "Lives, deaths and afterlives of interacting stars". The aim of this project is to study the impact of the rejuvenation process occurring during a first stable mass transfer on a later phase of common envelope evolution. To do so, we perform 3D hydrodynamics simulations of the common envelope evolution of a 18 $M_\odot$ red supergiant and a 1.4 $M_\odot$ companion. We compare two sets of simulations, one with a rejuvenated donor and one with a non-rejuvenated donor, to characterise the effect of the rejuvenation on the outcome of the common envelope phase. We find that rejuvenation does impact the speed of the inspiral, the shape of the ejecta and the amount of mass unbound from the envelope. In our simulations, taking rejuvenation into account resulted in a faster inspiral and less efficient envelope unbinding. It also yields a tighter envelope, which shows stronger asymmetries than in the case of a non-rejuvenated envelope.

*Keywords:* Common envelope binary stars (2156) — Common envelope evolution (2154) — Hydrodynamics (1963) — Hydrodynamical simulations (767) — Interacting binary stars (801)

## 1. INTRODUCTION

An important fraction of stars are found in binary systems (Abt & Levy 1976; Bonnell et al. 2004; Duchêne & Kraus 2013; Moe & Di Stefano 2017), especially massive stars (Mason et al. 2009; Sana & Evans 2010). These binary systems show a large variety of configurations, ranging from very wide systems with separation of thousands of AUs to binaries with periods of a few minutes. In the case of a close binary, the proximity of the two stars is such that they will likely interact via mass transfer and their evolution will strongly diverge from that of a single star (Podsiadlowski et al. 1992; Sana et al. 2012; Langer 2012; Smith 2014; De Marco & Izzard 2017). In particular, close binaries commonly go through phases of stable mass transfer through Roche Lobe overflow (RLOF). During this phase, the donor star overfills its Roche Lobe, and material leaves the potential well of the donor to be accreted by the companion, altering its structure in various ways (Packet 1981; Cantiello et al. 2007; Renzo & Götberg 2021). A main sequence (MS) star accretor with a convective core is expected to undergo a rejuvenation process during which its core expands and increases its hydrogen content through convective mixing (Hellings 1983). Besides increasing the lifetime of the accretor, this process also alters the structure of its core-envelope boundary (CEB) region. Recently, Renzo et al. (2023) found that the rejuvenation process lowers the binding energy of the CEB, which is of particular interest if the system later undergoes common envelope evolution (CEE) with the rejuvenated star as donor.

CEE is a phase of binary evolution during which the secondary star plunges in the envelope of a giant primary and orbit its core (Paczynski 1976; Ivanova et al.

Corresponding author: Camille Landri
camille.landri@utf.mff.cuni.cz

2013b). The drag excerced on the companion by the envelope causes the orbit to decay, transferring energy and angular momentum to the envelope and potentially unbinding it. The outcomes of CEE are still very uncertain: a successfully ejected envelope should lead to a short period binary that could emit gravitational waves, but if part of the envelope remains bound the binary might not survive. It could then merge as luminous red novae (Ivanova et al. 2013a; Pejcha 2020) or become a Thorne-Zýtkow object Thorne & Zytkow (1977). CEE is an important formation channel for close binaries, and while it has been extensively studied, it is still unclear which physical processes are involved in the ejection of the envelope.

Since the outcome of CEE strongly depends on the unbinding of the envelope, the fact that rejuvenation lowers the binding energy of the CEB is of particular interest when studying the outcome of CEE. The CEB is the region where most of the binding energy is stored, therefore a CEE with a rejuvenated donor might eject a larger part of the envelope and significantly influence the outcome of the CEE. This scenario is of interest for formation channels of binary black holes and neutron stars that expect a first phase of stable mass transfer before CEE (Tutukov & Yungelson 1993; Belczynski et al. 2016; Tauris et al. 2017). In such cases, the rejuvenation of the MS accretor during the first mass transfer phase could help unbinding its envelope when it takes the role of the giant donor during a later CEE.

In this paper, we aim to investigate how past rejuvenation of a CEE donor impacts the unbinding of the envelope during CEE. To do so, we perform 3D hydrodynamics simulations of the inspiral phase of the CEE with rejuvenated and non-rejuvenated donor models obtained by Renzo et al. (2023). We briefly describe the initial stellar models for the donor star as well as the setup of our hydrodynamics simulations in Section 2. We present our current results in Section 3 and present our preliminary conclusion in Section 4.

## 2. NUMERICAL METHODS

Our simulations make use of FLASH 4.5 (Fryxell et al. 2000; Dubey et al. 2008), an adaptive mesh refinement (AMR) hydrodynamics code. We use the directionally split piecewise parabolic method (PPM) solver supplied with FLASH together with the Helmholtz equation of state, parallel FFT-based multigrid Poisson solver (Ricker 2008; Daley et al. 2012), and a second-order leapfrog time integrator for particles. Simulations take place within a 3D Cartesian volume 72 AU on a side, with "diode" boundary conditions for hydrodynamics and isolated boundary conditions for the gravitational field.

To initialize each simulation, we begin with a 1D MESA model for the donor (described below). Since the star's actual core is very difficult to resolve, we replace it with a numerical core following a procedure similar to that described by Ohlmann et al. (2017). Given a choice of numerical core radius $r_c$, to the MESA model at this radius we join a solution of the modified Lane-Emden equation representing a gaseous polytrope in the potential of a uniform-density spherical core of mass $M_c$, which satisfies

$$\frac{d}{d\xi}\left(\xi^2\frac{d\theta}{d\xi}\right) + \xi^2(\theta^n + \theta_c^n) = 0 \ . \tag{1}$$

Here we adopt the customary definitions for the density and radius variables $\theta$ and $\xi$ via

$$\rho \equiv \rho_0\theta^n \ , \quad r \equiv \alpha\xi \ , \tag{2}$$

where $\rho_0$ is the central density, $n$ is the polytropic index, and $\alpha$ is the scale height. This equation differs from the normal Lane-Emden equation by one term involving

$$\theta_c^n \equiv \frac{M_c}{4\pi r_c^3\rho_0} \ . \tag{3}$$

The density $\rho(r_c)$ and pressure $P(r_c)$ are used to determine the polytrope's specific entropy $K \equiv P/\rho^\gamma$ and thus also $\alpha^2 = \frac{K(n+1)}{4\pi G}\rho_0^{1/n-1}$. The polytropic index $n$ is set using the adiabatic index reported by the equation of state at $r = r_c$ via $n = 1/[\gamma(r_c) - 1]$. Isotopic abundances are also matched and held constant throughout the polytrope. The core mass $M_c$ and polytrope central density $\rho_0$ are varied in a nested pair of bisection loops until a solution that matches the density and enclosed mass at $r_c$ is found. The part of the MESA model inside $r_c$ is replaced by the polytrope, and the derived core mass is used to initialize a collisionless particle at the center of the star. The companion star is also initialized as a particle but with mass $1.4M_\odot$.

The particles representing the numerical donor core and the companion interact only gravitationally with the gas. The interaction is determined by computing the acceleration due to the two cores in each mesh zone and storing it as an AMR variable that is added to the finite-differenced gas potential found with the Poisson solver. The acceleration of each core due to the gas is summed during this loop in such a way as to ensure momentum conservation. The donor core and companion also experience a mutual gravitational interaction. This method differs from the technique used in previous FLASH common envelope simulations and yields greatly improved

conservation properties, though because the gas gravitational acceleration is not explicitly conserved, and the time centering of the gas and particle update steps is not the same, we do not conserve momentum to within roundoff error. We monitor conservation in each of the runs and present these results in the Appendix.

Once the core properties have been determined, we interpolate the modified MESA model onto the center of the AMR grid and allow it to relax for 10 dynamical times. Outside the giant, the gas is initialized as a uniform "fluff" medium at rest with temperature and density set to approximately balance any outflow due unresolved pressure gradients at the stellar boundary (25000 K and $10^{-12}$ g cm$^{-3}$). During this period we damp the velocity field by multiplying all velocities by 0.9 at the end of each step. We then restart the simulation from a checkpoint file, turn off damping, and add the companion star, placing it on the $x$-axis at a separation $a_{\rm init}$ for which the Roche lobe radius (computed using the Eggleton (1983) approximation) equals the MESA model's stellar radius. These initial separations correspond to $843.92R_\odot$ (period 654.61 d) and $838.51R_\odot$ (period 641.08 d) for the rejuvenated and non-rejuvenated donors, respectively. The common envelope simulation is then run from this initial condition until the orbit stabilizes or the separation of the two cores becomes smaller than the sum of their radii ($2r_c$).

While the donor is not quite in equilibrium with the binary potential to begin with, because all runs begin with this setup we expect the differences between them to be mainly due to the differences in the donor model.

The AMR grid is refined by applying the default FLASH second-derivative criterion to the density and pressure and by requiring refinement of blocks containing any zone whose center is within $4r_c$ of a stellar core. We allow all blocks that contain a stellar core to refine to a higher maximum refinement level than those that do not. Convergence testing showed that, for the donor models considered in this paper, we required the numerical core radius to be at least 5 and preferably 10 times the smallest zone spacing in order to stably relax the donor. To avoid excessive refinement of the volume, we force derefinement of blocks whose maximum density is smaller than $10^{-10}$ g cm$^{-3}$ or which lie outside a distance of 18 AU from the center of the computational volume. Each AMR block contains $8^3$ zones, and the coarsest level of refinement contains $12^3$ blocks.

The initial stellar profiles of the donor used in this study are part of the models computed by Renzo et al. (2023) using MESA (version 15140, Paxton et al. 2011, 2013, 2015, 2018, 2019). We use their non-rotating 17.84 $M_\odot$ single star for the non-rejuvenated donor and their 15 $M_\odot$ accretor that reaches 17.41 $M_\odot$ after case-B mass transfer for the rejuvenated donor. Both donors have a radius of 500 $R_\odot$ and a metallicity of 0.10 $Z_\odot$, and have not started burning helium. In Figure 1 we show how the cumulative binding energy profiles of the two stellar models differ. The binding energy was calculated using

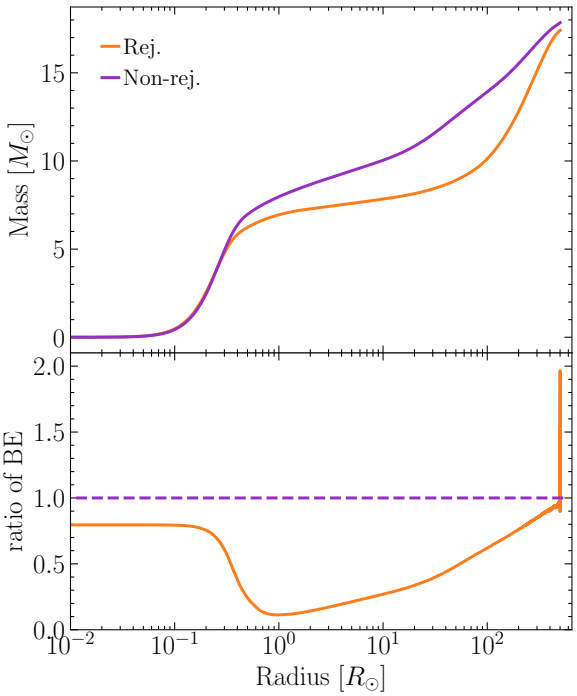


**Figure 1.** MESA stellar models for the rejuvenated (orange) and non-rejuvenated (purple) stars, assuming $\alpha_{th} = 1$. Top panel: Enclosed mass. Bottom panel: Ratio of the cumulative binding energy of the rejuvenated star to that of the non-rejuvenated star.

$$BE(m, \alpha_{th}) = -\int_m^M \left(-\frac{Gm'}{r(m')} + \alpha_{th} u(m')\right) dm' \ , \tag{4}$$

where $\alpha_{th}$ is the fraction of internal energy that can be used to unbind the envelope.

For each stellar model we performed runs at several different resolutions, varying the maximum level of refinement and the number of finest-level zones per numerical core radius. Table 2 summarizes the different simulations, and Figure 2 shows the density profiles after the replacement of the core for different resolutions, as well as the initial MESA density and composition profiles.

## 3. RESULTS

### 3.1. *Evolution of the binary*

We first examine the orbit of the binary during the CEE, to find out if it stabilises or if the stellar cores

**Table 1.** Simulations performed for this study.

| Donor | Core radius ($R_\odot$) | Min. cell size ($R_\odot$) | Core mass ($M_\odot$) | Envelope mass ($M_\odot$) |
|---|---|---|---|---|
| Rej. | 25 | 5.0 | 7.91 | 9.50 |
| | 25 | 2.5 | 7.91 | 9.50 |
| | 6.25 | 0.625 | 7.44 | 9.97 |
| Non-rej. | 25 | 5.0 | 10.26 | 7.58 |
| | 25 | 2.5 | 10.26 | 7.58 |
| | 6.25 | 0.625 | 9.12 | 8.72 |

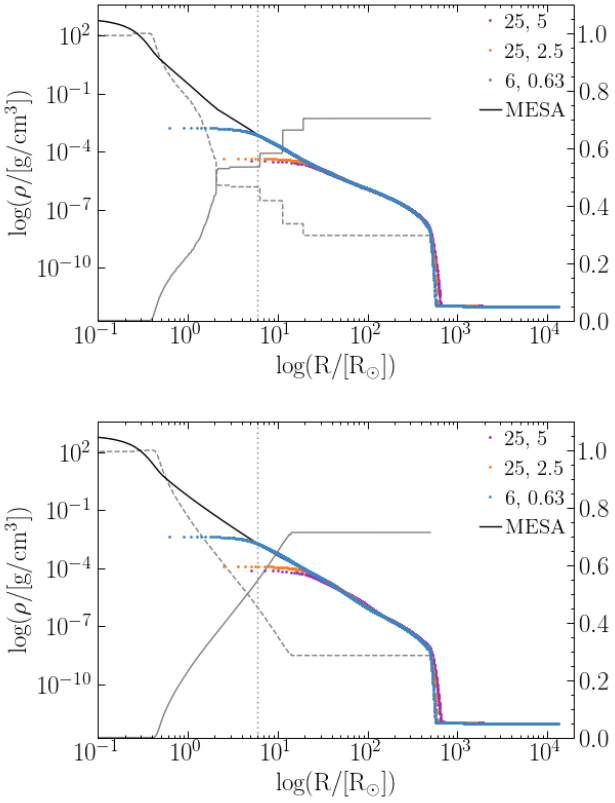


**Figure 2.** Density profiles of the donor at the start of the CEE. Runs are labeled using their numerical core radius and finest resolution. Upper panel: rejuvenated donor. Lower panel: non-rejuvenated donor. Colored dots represent the density profile for different resolutions and black lines represent the initial MESA profile. The gray solid and dashed lines show the fractions of H and He respectively. The gray dotted line represents the $25R_\odot$ core radius.

merge. The evolution of the separation of the binary is shown in Fig 3 for both rejuvenated and non-rejuvenated models. The separation of the binary can be separated in two phases: the orbit first slowly decays, then the inspiral starts and the separation decreases more rapidly. During this inspiral phase, we observe small variations

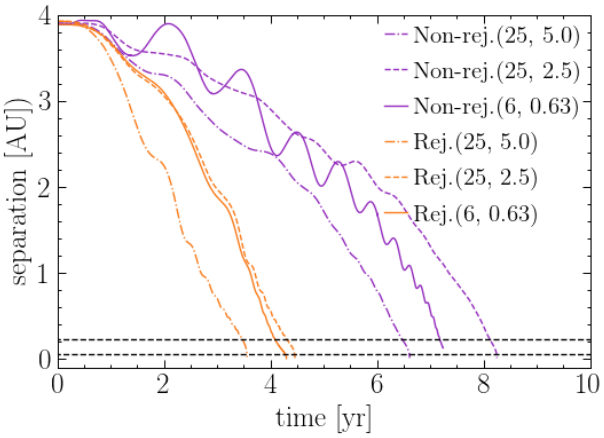


**Figure 3.** Evolution of the separation of the binary during the CEE for both rejuvenated (orange) and non-rejuvenated (purple) donors. Solid and dashed lines show the separation for (25, 2.5) and (25, 5.0) resolutions respectively. The black dashed lines denote where the separation is equal to the sum of the core radii $2R_{core} = 50R_\odot$ and $2R_{core} = 12R_\odot$.

in separation, which are due to the eccentricity of the orbit. From Fig 3 it is clear that the pace of both phases is affected by the resolution and the structure of the donor.

The slow shirking of the orbit lasts around a year for rejuvenated donors, while it takes between 4 and 6 years for the companion to plunge in the envelope of non-rejuvenated donors. Furthermore, the speed of the inspiral in the cases of a non-rejuvenated donor is slower than for rejuvenated envelopes. As a result, the binaries with rejuvenated donors reach the minimum separation between cores after 4 years in our current finest resolution, while the non-rejuvenated case takes more than 7 years.

The difference in resolution also strongly impacts the evolution of the binary separation, especially in the case of the non-rejuvenated donor. For the same core size, the runs with smaller minimum cell size show a slower inspiral. Additionally, while using a smaller core radius has little effect in the rejuvenated donor, the case Non-rej.(6, 0.63) shows strong differences with the other non-rejuvenated runs with larger core radii, In particular, it shows much stronger variations of separation due to eccentricity. This peculiar behaviour is indicative of issues in the simulations, which we therefore need to fix before drawing any real conclusion on the evolution of the high resolution systems.

Finally, none of our simulations show a stabilised orbit, the separation of the binaries reaches $2R_{core}$ before the orbit can become stable. This is not surprising considering the high mass ratio of the binary and the large

| Model | $M_{K+P}$ ($M_\odot$) | $M_{K+P+Th}$ ($M_\odot$) | Time ($t_{dyn}$) | final separation ($R_\odot$) |
|---|---|---|---|---|
| Rej.(25,5.0) | 0.18 | 0.51 | 12.78 | $\leq 50$ |
| Rej.(25,2.5) | 0.21 | 0.56 | 16.01 | $\leq 50$ |
| Rej.(6,0.63) | 0.17 | 0.53 | 15.43 | $\leq 12.5$ |
| Non-rej.(25,5.0) | 0.032 | 0.56 | 24.14 | $\leq 50$ |
| Non-rej.(25,2.5) | 0.005 | 0.59 | 30.12 | $\leq 50$ |
| Non-rej.(6,0.63) | 0.075 | 0.37 | 26.44 | $\leq 12.5$ |

**Table 2.** Summary of the results of the simulations.

size of our donor cores imposed even in the highest resolution runs. It is therefore not possible to conclude whether the stellar cores will merge or stabilise in a tight orbit, and we can only derive an upper limit on the final separation of the binary.

### 3.2. *Outflows*

We inspect the evolution of the shape of the outflow and the envelope during the simulation in Fig 4 and Fig 5. In both donor cases, we see the expected overdensities due to the inspiral of the companion, but the spirals appear slightly tighter in the case of the rejuvenated donor. From the slices of the equatorial plane in Fig 4 we see that the non-rejuvenated envelope has spread further by the end of the simulation than the rejuvenated envelope. The outflow also appears more spherically symmetric in the non-rejuvenated case. Additionally, the slices of the meridional plane of the envelope in Fig 5 show strong spherical asymmetries, with a large decrease in density around the polar axis. In particular, the matter distribution in the rejuvenated envelope appears very asymmetric with respect to the z-axis of the grid.

The differences in the symmetries and shape of the ejecta are partly due to the different speed at which the companion spirals in. In particular, a slower inspiral gives more time for the outflow to spread further, which explains why the non-rejuvenated envelope is much more extended at the end of the simulation. We will conduct further analysis of the mass distribution in the envelope in order to accurately define the impact of rejuvenation on the shape of the outflows.

### 3.3. *Mass loss*

Since all the binaries reach their minimum separation of $2R_{core}$ in our current results, a part of the inspiral is not resolved. Therefore, we can only find a lower limit to the total mass lost by the envelope during the CEE of our systems. In Fig 6 we show the amount of envelope mass lost in our simulations, where a parcel of matter is

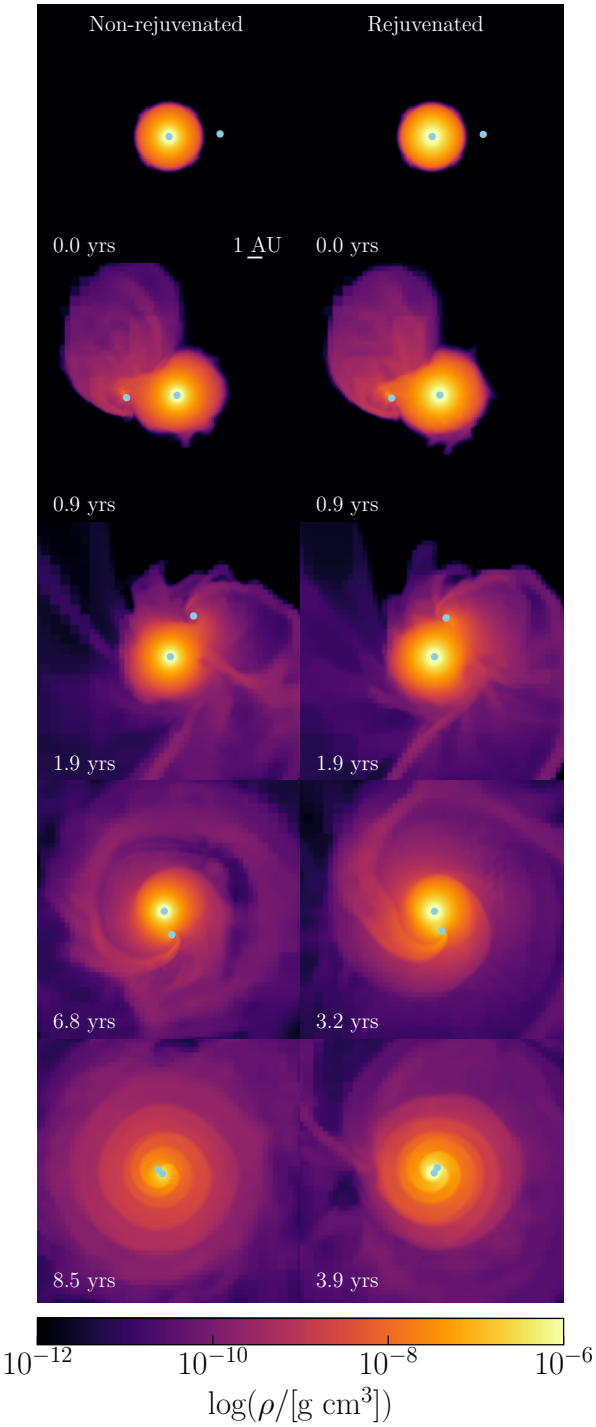


**Figure 4.** Snapshots of the Rej.(25, 2.5) and Non-rej.(25, 2.5) runs in the equatorial plane. Each panel shows a density slice at z=0 and is 20 by 20 A.U. The donor core and companion are denoted as grey points. Left panels: run with non-rejuvenated donor Non-rej.(25, 10.0). Bottom panels: run with rejuvenated donor Rej.(25, 10.0). First row: start of the run. Second and third row: first grazing of the envelope of the donor by the companion. Fourth row: core-companion separation is around 2 A.U. Fifth row: core-companion separation is 2 $R_{core}$.

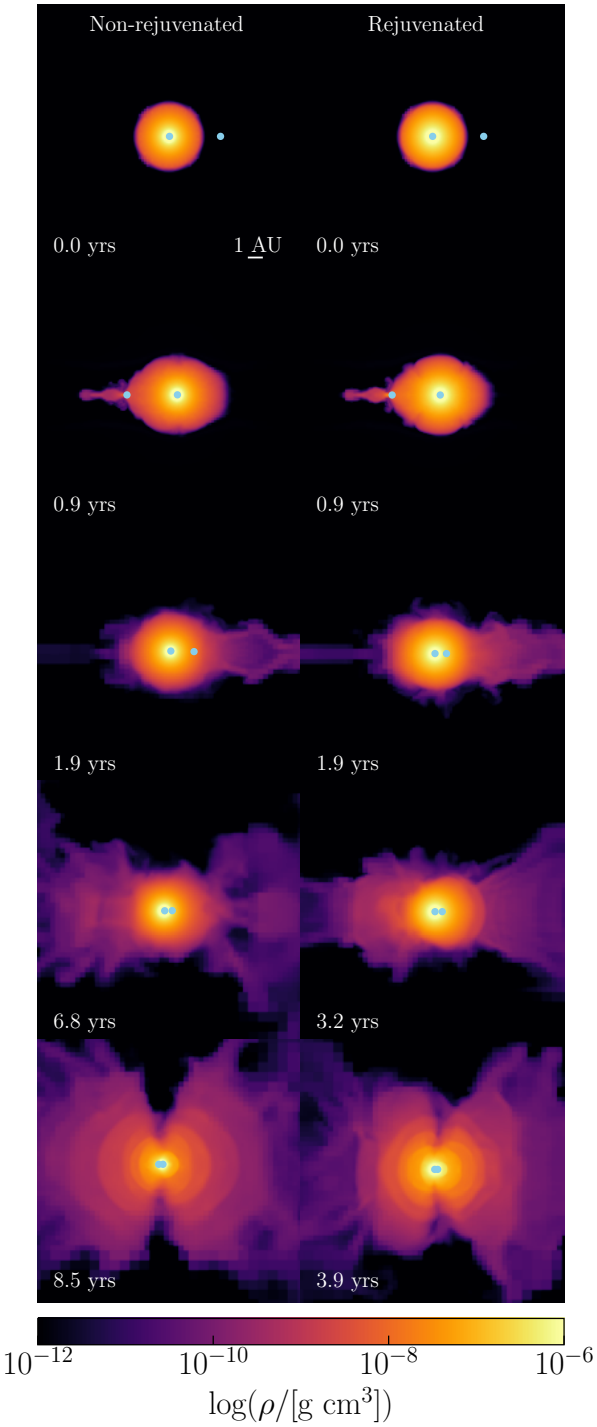


**Figure 5.** Same as Fig 4 but in the meridional plane. Each panel shows a density slice at y=0 and is 20 by 20 A.U. The donor core and companion are denoted as blue points. Top panels: run with rejuvenated donor Rej.(25, 10.0). Bottom panels: run with non-rejuvenated donor Non-rej.(25, 10.0). First and second column: first grazing of the envelope of the donor by the companion. Third column: core-companion separation is around 2 A.U. Fourth column: core-companion separation is 2 $R_{core}$.

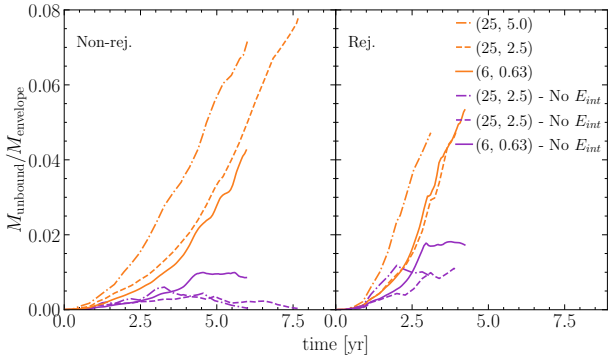


**Figure 6.** Evolution of the amount of unbound mass during the CEE for different resolution and donor model. Orange lines show the unbound mass considering a total energy calculated using only the potential and kinetic energy of each cell. Purple lines show the unbound mass considering a total energy calculated using the potential, kinetic and internal energy of each cell. Mass is considered unbound if its total energy is positive. Left panel: Simulations with a non-rejuvenated donor. Right panel: Simulations with a rejuvenated donor.

considered unbound if its total energy is positive. The total energy of the element is derived in two ways: by summing its potential, kinetic and internal energy, or by just considering its potential and kinetic energy. The former criterion implies that the internal energy of the gas is converted to kinetic energy.

We first note that similarly to the evolution of the binary separation, only the mass loss of the non-rejuvenated donor is strongly impacted by the change of resolution. In fact, Non-rej.(6, 0.63) shows a 40% decrease in mass loss compared to the lower resolution runs, but a 100% increase when considering the more conservative energy criterion. Furthermore, the rejuvenation of the donor also affects the mass loss: the rejuvenated giant loses 0.055 $M_{env}$ while the non-rejuvenated one loses 0.075 $M_{env}$ when considering the less conservative formula for mass loss. While both donor models do not yield great mass loss, the mass loss increases by 35% between the rejuvenated and non-rejuvenated cases.

Interestingly, this trend reverses when considering the more conservative criterion for mass loss. The mass loss in the rejuvenated systems reaches $0.02 M_{env}$ against $0.01 M_{env}$ in the non-rejuvenated case, effectively showing a 100% increase when taking rejuvenation into account. The overall mass loss greatly decreases when considering only the kinetic and potential contributions to the total energy of the gas, indicating that internal energy is not efficiently converted to kinetic energy. Additionally, the amount of mass lost in non-rejuvenated envelopes significantly decreases after half of the inspiral

has passed, suggesting that part of the ejected envelope slows down and becomes bound again.

Overall, the total mass unbound by the CEE is low, which is consistent with the cores merging. However the resolution of our simulation is too low to resolve the late phase of the inspiral, which could lead to a higher mass loss rate and potentially the stabilisation of the binary orbit.

## 4. DISCUSSION AND CONCLUSION

We have performed 3D hydrodynamics simulations of CEE using rejuvenated and non-rejuvenated donor models. We have found that rejuvenation does impact the speed of the inspiral, the shape of the ejecta and the amount of mass loss.

In our simulations, taking rejuvenation into account resulted in a faster inspiral and less efficient envelope unbinding. This is likely due to the increase of density in the outer envelope of the rejuvenated donor (see upper panel of Fig 1), which strengthens the drag on the companion when it starts to plunge in the envelope. A more thorough analysis of the results of the simulations will be performed to characterise more accurately the impact of rejuvenation. In particular, we will study the morphology of the ejecta and the distribution of unbound mass in more details.

We note that our current simulations have relatively large core sizes that do not allow to resolve the region close to the CEB, where the difference in binding energy is supposed to be the strongest. Therefore, simulations with smaller core sizes and higher resolution are needed to study the full impact of rejuvenation.

Finally, As mentioned in Section 3.1, the highest resolution run of the non-rejuvenated envelope Non-rej.(6, 0.63) shows peculiar results, indicating issues with our simulations. Specifically, we have found problems in the setup of the binary systems, during which the gas was mistakenly set in co-rotation with the binary, as well as issues with the mapping of the MESA models to the FLASH grid. These issues will be corrected and the simulations reran before submitting the paper based on this project.

This project was initiated at the 2023 Kavli Summer Program in Astrophysics held at the Max Planck Institute for Astrophysics (MPA). We thank MPA and the Kavli Program for their support. FLASH was developed and is maintained largely by the DOE-supported Flash Center for Computational Science at the University of Chicago (now at the University of Rochester). Simulations were performed using computational resources at MPA and Charles University.

*Software:* FLASH (Fryxell et al. 2000; Dubey et al. 2008) yt (Turk et al. 2011) Matplotlib (Hunter 2007) NumPy (Harris et al. 2020)

## REFERENCES

Abt, H. A., & Levy, S. G. 1976, The Astrophysical Journal Supplement Series, 30, 273, doi: 10.1086/190363

Belczynski, K., Holz, D. E., Bulik, T., & O'Shaughnessy, R. 2016, Nature, 534, 512, doi: 10.1038/nature18322

Bonnell, I. A., Vine, S. G., & Bate, M. R. 2004, Monthly Notices of the Royal Astronomical Society, 349, 735, doi: 10.1111/j.1365-2966.2004.07543.x

Cantiello, M., Yoon, S. C., Langer, N., & Livio, M. 2007, Astronomy and Astrophysics, 465, L29, doi: 10.1051/0004-6361:20077115

Daley, C., Vanella, M., Dubey, A., Weide, K., & Balaras, E. 2012, Concurrency and Computation: Practice and Experience, doi: 10.1002/cpe

De Marco, O., & Izzard, R. G. 2017, Publications of the Astronomical Society of Australia, 34, e001, doi: 10.1017/pasa.2016.52

Dubey, A., Reid, L. B., & Fisher, R. 2008, Physica Scripta, T132, 014046, doi: 10.1088/0031-8949/2008/T132/014046

Duchêne, G., & Kraus, A. 2013, Annual Review of Astronomy and Astrophysics, 51, 269, doi: 10.1146/annurev-astro-081710-102602

Eggleton, P. P. 1983, The Astrophysical Journal, 268, 368, doi: 10.1086/160960

Fryxell, B., Olson, K., Ricker, P., et al. 2000, The Astrophysical Journal Supplement Series, 131, 273. http://iopscience.iop.org/0067-0049/131/1/273

Harris, C. R., Millman, K. J., Walt, S. J. v. d., et al. 2020, Nature, 585, 357, doi: 10.1038/s41586-020-2649-2

Hellings, P. 1983, Astrophysics and Space Science, 96, 37, doi: 10.1007/BF00661941

Hunter, J. D. 2007, Computing in Science & Engineering, 9, 90, doi: 10.1109/MCSE.2007.55

Ivanova, N., Justham, S., Nandez, J. L. A., & Lombardi Jr, J. C. 2013a, Science, 339, 433, doi: 10.1126/science.1225540

Ivanova, N., Justham, S., Chen, X., et al. 2013b, The Astronomy and Astrophysics Review, 21, 59, doi: 10.1007/s00159-013-0059-2

Langer, N. 2012, Annual Review of Astronomy and Astrophysics, 50, 107, doi: 10.1146/annurev-astro-081811-125534

Mason, B. D., Hartkopf, W. I., Gies, D. R., Henry, T. J., & Helsel, J. W. 2009, The Astronomical Journal, 137, 3358, doi: 10.1088/0004-6256/137/2/3358

Moe, M., & Di Stefano, R. 2017, The Astrophysical Journal Supplement Series, 230, 15, doi: 10.3847/1538-4365/aa6fb6

Ohlmann, S. T., Röpke, F. K., Pakmor, R., & Springel, V. 2017, Astronomy and Astrophysics, 599, A5, doi: 10.1051/0004-6361/201629692

Packet, W. 1981, Astronomy and Astrophysics, 102, 17. https://ui.adsabs.harvard.edu/abs/1981A&A...102...17P

Paczynski, B. 1976, 73, 75. https://ui.adsabs.harvard.edu/abs/1976IAUS...73...75P

Paxton, B., Bildsten, L., Dotter, A., et al. 2011, The Astrophysical Journal Supplement Series, 192, 3, doi: 10.1088/0067-0049/192/1/3

Paxton, B., Cantiello, M., Arras, P., et al. 2013, Modules for Experiments in Stellar Astrophysics (MESA): Giant Planets, Oscillations, Rotation, and Massive Stars, arXiv e-print 1301.0319. http://arxiv.org/abs/1301.0319

Paxton, B., Marchant, P., Schwab, J., et al. 2015, The Astrophysical Journal Supplement Series, 220, 15, doi: 10.1088/0067-0049/220/1/15

Paxton, B., Schwab, J., Bauer, E. B., et al. 2018, The Astrophysical Journal Supplement Series, 234, 34, doi: 10.3847/1538-4365/aaa5a8

Paxton, B., Smolec, R., Schwab, J., et al. 2019, The Astrophysical Journal Supplement Series, 243, 10, doi: 10.3847/1538-4365/ab2241

Pejcha, O. 2020, Proceedings of the International Astronomical Union, 16, 159, doi: 10.1017/S174392132200059X

Podsiadlowski, P., Joss, P. C., & Hsu, J. J. L. 1992, The Astrophysical Journal, 391, 246, doi: 10.1086/171341

Renzo, M., & Götberg, Y. 2021, The Astrophysical Journal, 923, 277, doi: 10.3847/1538-4357/ac29c5

Renzo, M., Zapartas, E., Justham, S., et al. 2023, The Astrophysical Journal, 942, L32, doi: 10.3847/2041-8213/aca4d3

Ricker, P. M. 2008, The Astrophysical Journal Supplement Series, 176, 293. http://iopscience.iop.org/0067-0049/176/1/293

Sana, H., & Evans, C. J. 2010, Proceedings of the International Astronomical Union, 6, 474, doi: 10.1017/S1743921311011124

Sana, H., de Mink, S. E., de Koter, A., et al. 2012, Science, 337, 444, doi: 10.1126/science.1223344

Smith, N. 2014, Annual Review of Astronomy and Astrophysics, 52, 487, doi: 10.1146/annurev-astro-081913-040025

Tauris, T. M., Kramer, M., Freire, P. C. C., et al. 2017, The Astrophysical Journal, 846, 170, doi: 10.3847/1538-4357/aa7e89

Thorne, K. S., & Zytkow, A. N. 1977, The Astrophysical Journal, 212, 832, doi: 10.1086/155109

Turk, M. J., Smith, B. D., Oishi, J. S., et al. 2011, The Astrophysical Journal Supplement Series, 192, 9, doi: 10.1088/0067-0049/192/1/9

Tutukov, A. V., & Yungelson, L. R. 1993, Monthly Notices of the Royal Astronomical Society, 260, 675, doi: 10.1093/mnras/260.3.675